JOURNAL OF MECHANICS OF CONTINUA AND MATHEMATICAL SCIENCES
www.journalimcms.org

ISSN (Online) : 2454 -7190 Vol.-20, No.-12, December (2025) pp 78-92 ISSN (Print) 0973-8975

ENHANCING THE FLEXURAL STRENGTH OF HIGH-PERFORMANCE CONCRETE BEAMS USING BASALT FIBER REINFORCED POLYMER

Mohammad Hematibahar[1], Mosarof SK[2], Dahi S. Vanus[3]
Makhmud Kharun[4]

[1]Department of Architecture, Restoration and Design, RUDN University, Moscow, Russia.

ANO "SAFAS", Moscow, Russia.

[2,3,4]Department of Reinforced Concrete & Masonry Structures, Moscow State University of Civil Engineering, Moscow, Russia.

Email : [1]eng.m.hematibahar1994@gmail.com, [2]mosarofsekh72@gmail.com
[3]dahiws@gmail.com, [4]miharun@yandex.ru

Corresponding Author: **Makhmud Kharun**

https://doi.org/10.26782/jmcms.2025.12.00006

(Received: July 06, 2025; Revised: November 07, 2025; November 22, 2025)

Abstract

This study investigates the enhancement of flexural strength of high-performance concrete (HPC) beams using basalt fiber reinforced polymer (BFRP) embedded internally at different depths. Four types of beam samples were tested: BFRP placed directly on the bottom (CB0), and BFRP placed at 0.75 cm (CB0.75), 1.25 cm (CB1.25), and 2.25 cm (CB2.25) from the bottom. The concrete mixture, which resembled ultra-high-performance concrete, included binder, fine and coarse aggregates, glass powder, microsilica, and a plasticizer. The results showed that BFRP significantly improved the flexural strength and ductility compared to the control samples without BFRP reinforcement. Optimum performance was achieved by placing the BFRP at 1.25 cm from the bottom (CB1.25), which demonstrated an increase in flexural strength by 1088% (653 kN/m^2) and displacement by 0.225 mm compared to the control samples, indicating a balanced distribution of strength and stress. Large distances (e.g., CB2.25) reduce the effectiveness, highlighting the importance of BFRP proximity to tension zones.

Keywords: Basalt Fiber Reinforced Polymer, Flexural Strength, Ductility, High-Performance Concrete, Reinforced Concrete Beam.

I. Introduction

Various researchers are trying to improve the mechanical and physical properties of concrete by adding or attaching various materials to concrete. In recent years, basalt has become one of the contenders for fibrous reinforcement of composites due to its promising physical, chemical, and mechanical properties, as

well as good technological characteristics and cost-effectiveness of the corresponding production technologies [XIII], [XVII], [XIX], [XXII]. Adding fiber is a way to improve the mechanical properties of concrete. For example, Kharun et al. [XXI] found that adding 1.2% basalt fibers maximized the flexural strength of concrete, while 0.9% basalt fibers maximized the compressive strength. In another example, Hematibahar et al. [XX] also found that 1.2% basalt fibers can improve the mechanical properties of concrete, such as flexural and tensile strength. Some studies attempt to improve the mechanical properties of concrete by adding chemical powder [I], [VI]. For example, Beskopylny et al. [VII] added coffee grounds (CG) and peanut shell ash (PSA) to cementitious material to improve mechanical properties. They found that the addition of 0.1–0.3% CG and PSA improved the mechanical properties of cementitious materials.

There are many types of concrete reinforcement, one of which is adding a 3D printed reinforced pattern to the concrete [IX], [XV], [XVI]. For example, Hematibahar et al. [XVIII] optimized honeycomb, 3D honeycomb, grid, and triangle as 3D printed reinforcement for concrete. They found that the best sample was the honeycomb one, with rates of 76% and 118% compared to the control sample. In another example, Hematibahar et al. [XIV] compared 3D printed reinforced truss and shell structures and found that patterning was a parameter for improving mechanical properties such as flexural strength. Another example of concrete reinforcement is fiber-reinforced polymer (FRP) as a coating and reinforcement to improve the mechanical properties of concrete [II], [V], [XI], [X]. The use of external FRP as a concrete coating and repair has several advantages, including cost effectiveness and high ductility [V]. Some research shows that two layers of FRP have a greater impact on mechanical properties [XI]. Some studies mention that with high dosage of FRP, the mechanical properties of the concrete structure are improved [X]. In general, FRP is used to improve the mechanical properties of concrete, such as compressive, tensile, and flexural strength.

The flexural strength of a load-bearing beam is its ability to resist deformation and failure under bending loads. This is an important mechanical property, especially in structural design, which determines how much force a beam can withstand before failure. The ductility of a load-bearing beam is its ability to undergo significant inelastic deformation (bending or straining beyond the elastic limit) before failure, which provides a warning before failure. This is an important structural design factor, especially in seismic areas, as it allows a structure to absorb energy and redistribute forces, preventing sudden collapse.

Chen et al. [VIII] investigated the effects of different BFRP wrapping patterns, U-jacket anchorage, and epoxy adhesives on the flexural capacity of reinforced concrete beams. It was found that the use of U-jacket anchorage could increase the load-bearing capacity by up to 37.8%. The authors concluded that the use of inclined U-jackets is more efficient than vertical U-jackets, with the load-bearing capacity increasing up to 55.2%. Saribiyik et al. [XXIII] studied the effects of BFRP composite and wrapping methods on the shear strength of reinforced concrete beams. They found that the shear strength of reinforced concrete beams with BFRP

composites increased by 43–100%; the best results were obtained using a fully wrapped configuration among other configurations.

The experimental study presented in this article was conducted to investigate and evaluate the flexural strength and ductility of high-performance concrete (HPC) beams with basalt fiber reinforced polymer (BFRP).

II. Material and Methods

Material

Experimental study was conducted with the following composition: Portland cement CEM I 42.5 N as a binder, sand with a fineness modulus of 2.7 as a fine aggregate, granite crushed stone of fraction 7–14 mm as a coarse aggregate, glass powder as a filler, microsilica as a organo-mineral additive, SikaPlast®Concrete in liquid form as a plasticizer to improve the workability of concrete, and water for mixing (Table 1).

Table 1: Composition of concrete mixture.

Cement (kg/m^3)	Fine Aggregate (kg/m^3)	Coarse Aggregate (kg/m^3)	Glass Powder (kg/m^3)	Microsilica (kg/m^3)	Plactiziter (l/m^3)	Water (l/m^3)
550	1100	350	200	100	20	230

Sample Making and Research Method

To minimize sample variation, a process of creating identical samples was used in all tests.

The coarse aggregate (crushed stone) was pre-immersed in water for 24 hours before mixing, then removed from the water and placed on a sieve for 2 hours to dry out the water to achieve a nearly dry surface condition. All powdered materials (Portland cement, micro silica, and glass powder) were thoroughly mixed in a concrete mixer until a uniform color was obtained, after which fine and coarse aggregates (sand and crushed stone) were added to the resulting powder mixture. Liquid materials (SikaPlast®Concrete and water) were mixed in a separate container. This liquid substance was then added to the dry mixture and thoroughly mixed in the concrete mixer until a homogeneous mixture was obtained.

Control samples measuring 100x100x100 mm^3 for testing the compressive strength of HPC were produced. To test the beams, basalt fiber polymer fabric (Figure 1) was placed in the form measuring 400x100x100 mm^3 in two layers, then HPC was poured inside the form. Control samples CB for flexural strength and ductility tests were produced without BFRP. Four types of HPC beams with BFRP were tested in this study:

- CB0: HPC beam with BFRP placed directly on the bottom of the form;
- CB0.75: HPC beam with BFRP placed at 0.75 cm from the bottom of the form;
- CB1.25: HPC beam with BFRP placed at 1.25 cm from the bottom of the form;
- CB2.25: HPC beam with BFRP placed at 2.25 cm from the bottom of the form.

Fig. 1. Basalt fiber polymer fabric.

The samples were placed in water at 20–22 °C for 28 days to cure. The HPC cubes were tested according to ASTM C109 [III], and for the flexural test, the three-point bending test was carried out according to GB/T 17671 [XII]. Experimental studies were conducted on a hydraulic press with a force of up to 1500 kN during compression testing and up to 150 kN during flexural testing (Figure 2).

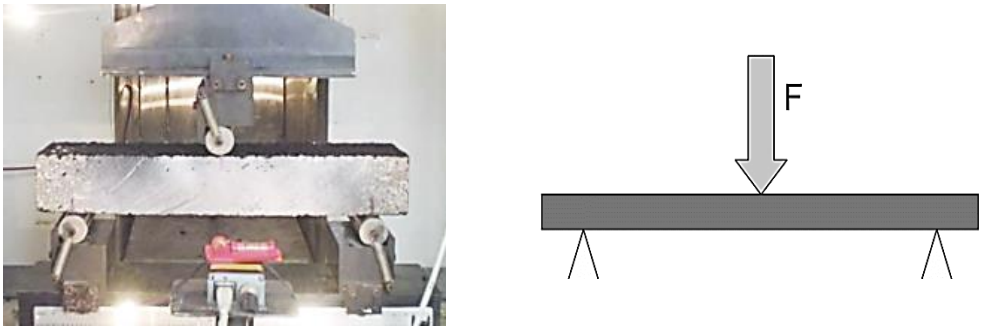

Fig. 2. Beam under flexural test.

Polynomial Prediction of Flexural Strength

A polynomial equation is used to find the flexural load-displacement curve. Equation (1) illustrates the polynomial formula [XX]:

$$y_{(x)} = a_n x^n + a_{n-1} x^{n-1} + a_{n-2} x^{n-2} + \cdots + a_2 x^2 + a_1 x^1 + a_0 \qquad (1)$$

where a is the coefficient of the polynomial function; a_n, a_{n-1}, a_{n-2}, …, a_2, a_1, a_0 are the coefficients of the polynomial (constant values); x is the variable; n is a non-negative integer, representing the highest power of x (degree of the polynomial); $y_{(x)}$ is a variable that depends on x.

In this study, second-degree polynomial regression was used to model the relationship between displacement and flexural load in HPC beams with BFRP. The analysis was performed using the Python's scikit-learn library, where the displacement values were transformed into polynomial features to account for nonlinear behavior. The model coefficients were optimized to match the experimental data, resulting in a prediction curve that accurately reflects the load-displacement

response. This approach allowed us to quantify the increase in flexural strength in different BFRP configurations, providing a mathematical basis for comparing performance trends.

III. Results and Discussion

Compressive Strength Test

The compressive strength of the HPC cube was 67 MPa (Figure 3). According to Figure 3, there is a sharp drop after reaching the maximum stress (67 MPa), which is typical for concrete. HPC samples can withstand a strain of about 0.013 before they fail. A curve without a clear yield zone exhibits elastic behavior up to the point of failure.

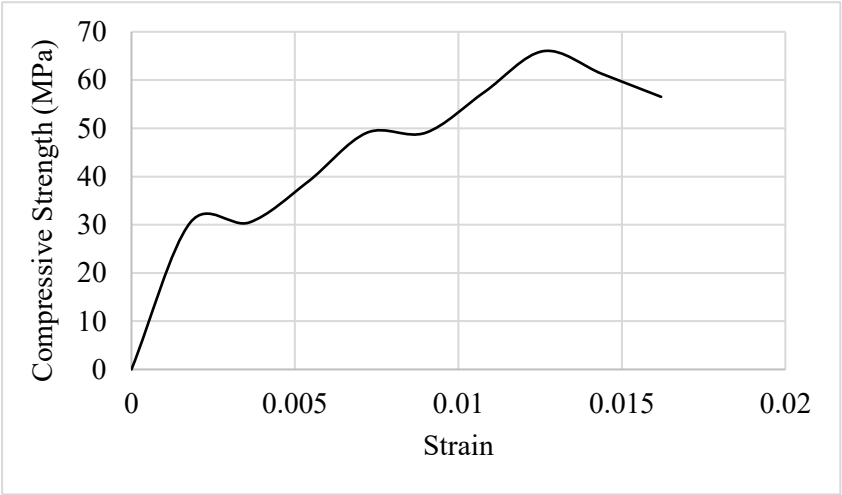

Fig. 3. Compressive stress-strain test.

Flexural Strength and Ductility Tests

Figure 4 shows the load-displacement of control samples CB. In this figure, the graph shows an almost linear relationship between displacement and flexural strength over a small range of variation, indicating the elastic behavior of the material. A sharp drop in strength after reaching the maximum load indicates brittle behavior of the samples, which is usually observed in concrete. The samples undergo a displacement of approximately 0.009 mm and then fail, indicating little deformation before failure. Due to the absence of BFRP, the strength and ductility of the samples are low, and their behavior depends entirely on the concrete matrix.

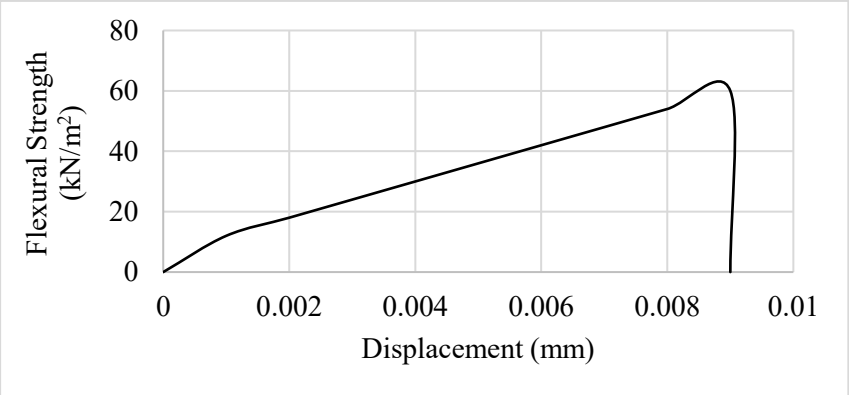

Fig. 4. Load-Displacement of Control Samples (CB).

Figure 5 shows the load-displacement of sample CB0. Adding BFRP to the bottom of the HPC beam significantly increased the flexural strength. The CB0 beams exhibit large deformation resistance (up to 0.12 mm) before failure, indicating improved ductility. In contrast to the control samples CB, the strength loss after reaching the maximum load is more gradual, indicating a more ductile behavior. The maximum displacement before failure is greater than that of the control samples CB, indicating better performance of the BFRP. The use of BFRP has simultaneously increased the strength and ductility of the HPC beam.

The addition of BFRP at 0.75 cm from the bottom of the HPC beam significantly increased the flexural strength compared to not only the control samples CB but even the samples CB0 (Figure 6). Unlike the control samples CB, which showed a sharp drop in strength, specimens CB0 and CB0.75 exhibit a softer deformation resistance after reaching the maximum load, indicating that BFRP is effective in supporting post-cracking stresses. The maximum displacement of samples CB0.75 reached 0.15 mm, which is an increase compared to samples CB0 (0.12 mm). The BFRP layer at a distance from the HPC bottom resulted in better stress distribution and prevented sudden rupture. The flexural strength of samples CB0.75 is at least 10–15% higher than samples CB0. Placing the BFRP at a distance of 0.75 from the bottom allowed for a better balance between strength and ductility. This is an ideal option for structures that must withstand dynamic loads or large deformations.

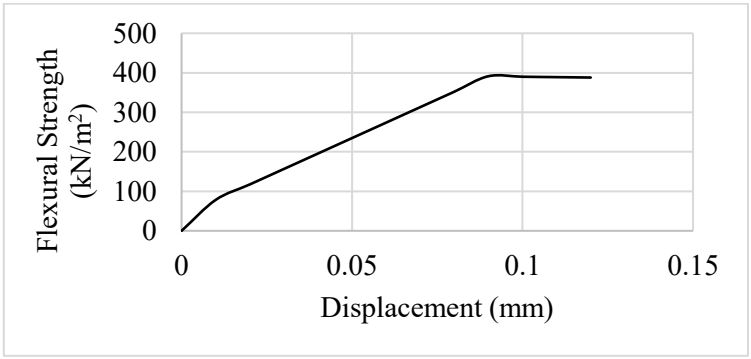

Fig. 5. Load-Displacement of CB0.

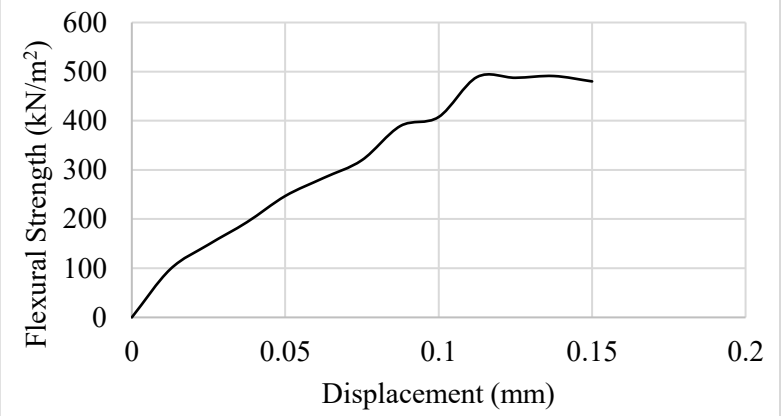

Fig. 6. Load-Displacement of CB0.75.

Figure 7 shows that placing BFRP at 1.25 cm from the bottom of the HPC beam reduces the effectiveness of the BFRP reinforcement, and the flexural strength is approximately 15–20% lower than that of the samples CB0.75. The maximum displacement increases to 0.225 mm, indicating higher flexibility. The flexural strength resistance in the direction of maximum load occurs more smoothly than in the control samples CB and even better than in the samples CB0.75. The greater distance of BFRP from the underlying surface reduces its ability to limit cracks and withstand tensile stresses. The flexural strength and deformation resistance of samples CB1.25 are approximately 85–90% higher than that of CB0.75. This option is suitable for higher loads or cases where large deformations are allowed.

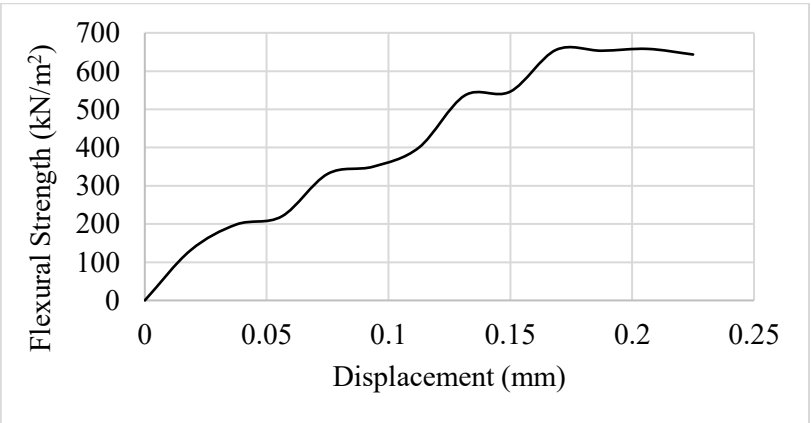

Fig. 7. Load-Displacement of CB1.25.

Figure 8 shows the load-displacement of sample CB2.25. When BFRP is placed at 2.25 cm from the bottom of the HPC beam, the flexural strength is reduced compared with CB0, CB0.75, and CB1.25, but deformation resistance is higher than CB0 and CB0.75.

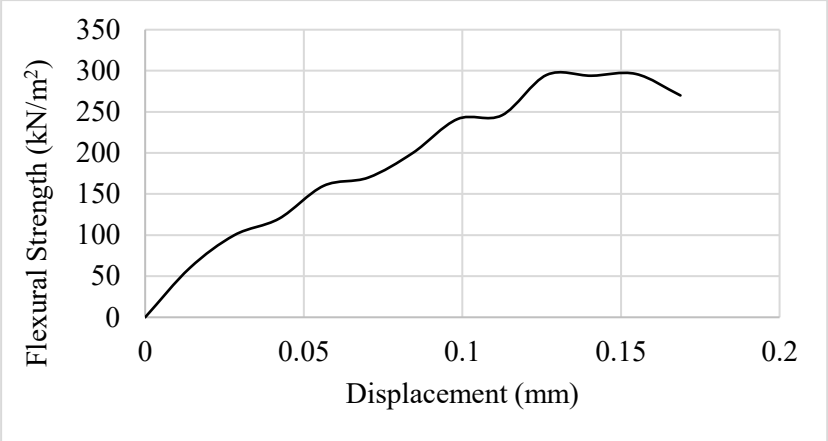

Fig. 8. Load-Displacement of CB2.25.

The results show that placing BFRP at a distance of 1.25 from the bottom of the HPC beam provides the best performance, while larger or smaller distances may result in reduced strength or unexpected behavior (Table 2).

Table 2: Flexural Strength and Maximum Displacement of Samples.

Samples	Maximum Flexural Strength (kN/m^2)	Maximum Displacement (mm)
Control Samples CB	60	0.009
CB0	391	0.12
CB0.75	487	0.15
CB1.25	653	0.225
CB2.25	293	0.16

The control samples CB with a flexural strength of 60 kN/m^2 and a maximum displacement of 0.009 mm exhibit completely brittle behavior and low load-bearing capacity, which is typical of unreinforced concrete. In samples CB0, the flexural strength reached 391 kN/m^2 (an increase of 650%), and the displacement reached 0.12 mm, indicating the significant effect of BFRP in simultaneously improving the flexural strength and ductility. The most optimal characteristics are demonstrated by the samples CB1.25 with a flexural strength of 653 kN/m^2 and a displacement of 0.225 mm, since the appropriate placement of BFRP resulted in a more efficient distribution of stresses and increased efficiency. In samples CB2.25, the flexural strength decreased to 293 kN/m^2, confirming the negative effect of the large distance of BFRP from the tensile zone. In general, a smaller distance of BFRP to the bottom (up to 1.25 cm) leads to an increase in flexural strength and ductility, but a larger distance (for example, 2.25 cm) leads to a sharp decrease in performance characteristics. For structures subject to heavy loads, the optimal distance from BFRP to the bottom is considered to be 1.25 cm, since this ensures a good balance between flexural strength and ductility.

Polynomial Strength

The flexural strength was calculated using polynomial regression and Python programming. Figure 9 (a – e) shows the flexural load-displacement and flexural strength, respectively, and presents the polynomial regression curves for the load-displacement behavior of HPC beams with BFRP, comparing the control samples with four reinforcement configurations (CB0, CB0.75, CB1.25, CB2.25). Each subplot illustrates experimental data points (scatter) next to the fitted quadratic curve, highlighting the nonlinear relationship between displacement and flexural load. The curves demonstrate how the placement of BFRP affects the mechanical properties, with sample CB1.25 demonstrating the optimum balance of flexural strength and ductility.

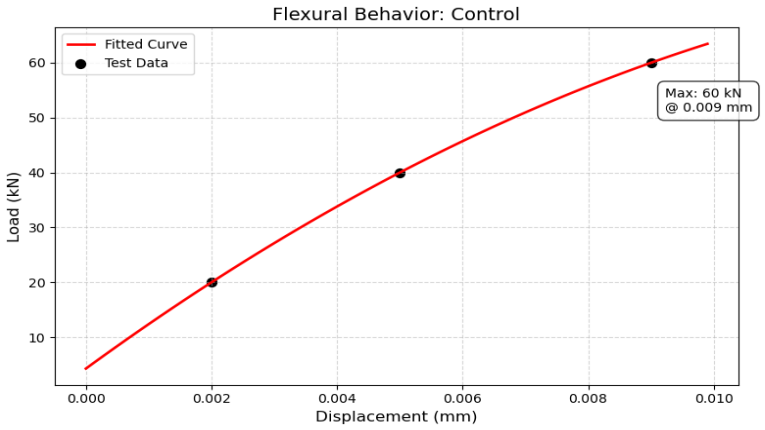

(a)

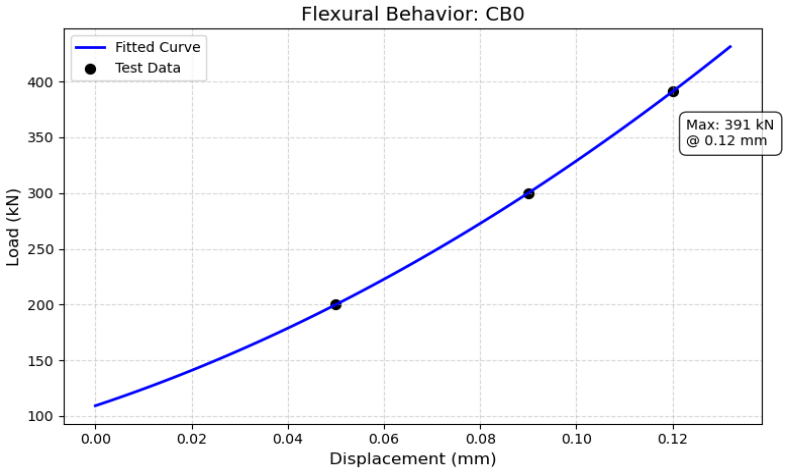

(b)

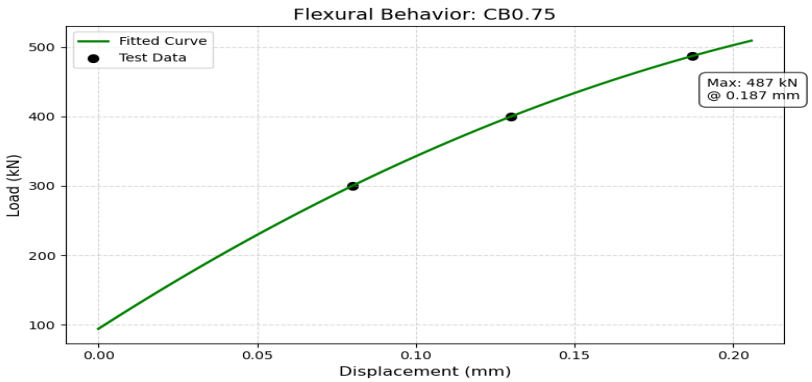

(c)

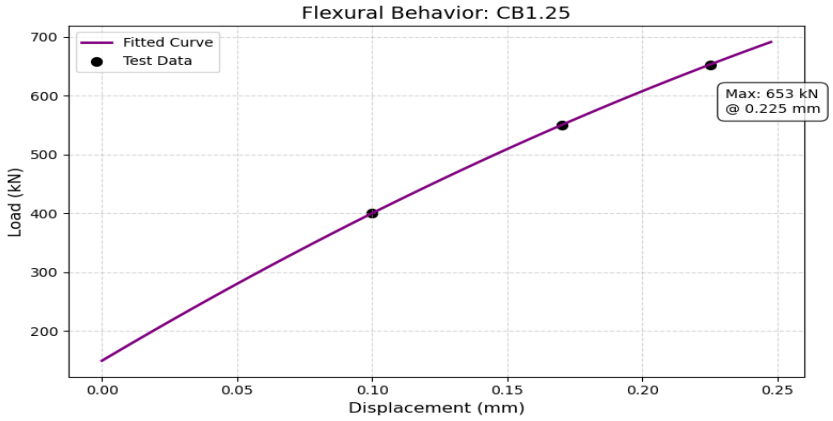

(d)

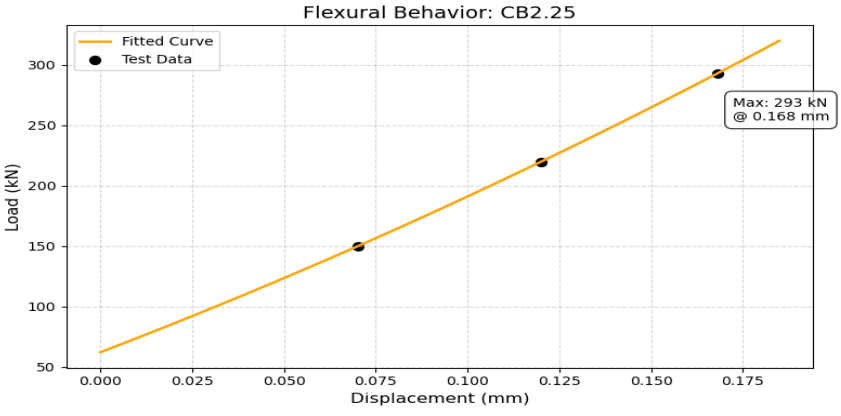

(e)

Fig. 9. Prediction of Flexural Strength:
(a) control samples CB, (b) CB0, (c) CB0.75, (d) CB1.25, (e) CB2.25.

The plots show clear behavioral shifts: the control specimen (a) shows a steep linear decline (brittle failure), while beams (b – e) with BFRP show a gradual decline after the peak (ductile failure). Subplot (c) for CB1.25 exhibits the highest peak load (653 kN) and increased displacement (0.225 mm), as validated by the close polynomial fit of the curve. The annotations focus on critical points such as maximum load and failure displacement, which support the study's conclusion that the proximity of the BFRP reinforcement to the tensile zone (1.25 cm) maximizes the design's performance.

The polynomial curves showed a clear agreement with the experimental results, especially for the samples with optimal BFRP placement (e.g., samples CB1.25). Regression analysis showed that the proximity of BFRP to the tensile zone (depth 1.25 cm) maximizes both flexural strength (653 kN/m^2) and ductility (displacement 0.225 mm). Deviations in samples CB1.25 and samples CB2.25 revealed sensitivity to reinforcement placement. The robustness of the model was confirmed by its ability to reproduce the brittle-ductile transition, highlighting its usefulness in the design of BFRP-reinforced structures to achieve target mechanical properties.

Scanning Electron Microscopy (SEM) Result

BFRP fabrics provide good adhesion to the concrete matrix due to their uniform fiber structure and fabric texture. SEM images in Figure 10 show that the basalt fibers are arranged regularly and have a uniform surface; this arrangement increases the contact area and therefore improves the efficiency of the fibers in transmitting stress. The structure of these fibers allows stress to be distributed across different areas of the fibers and prevents the formation of stress concentrations that typically lead to cracking.

Microscopic examination at 1 μm and 20 μm scales shows that in the contact areas between basalt fibers and cement paste, the matrix has penetrated well into the BFRP fabric. This penetration creates mechanical bonding and increases adhesion between the BFRP and concrete. This plays a key role in improving the flexural performance, since after the initial cracking of the concrete, the BFRP fabric mesh takes on the tensile load and prevents crack propagation.

According to the results presented in Figure 10, basalt fibers have a relatively rough and uneven surface due to their fabric structure, which increases internal friction and improves adhesion in the cement matrix. This structure improves the post-cracking behavior and increases the ductility of HPC beams reinforced with BFRP. Thus, the fabric nature of BFRP not only affects the improvement of flexural capacity but also changes the behavior of the structure from brittle to semi-rigid or even viscous, which is also clearly visible in the results of bending tests.

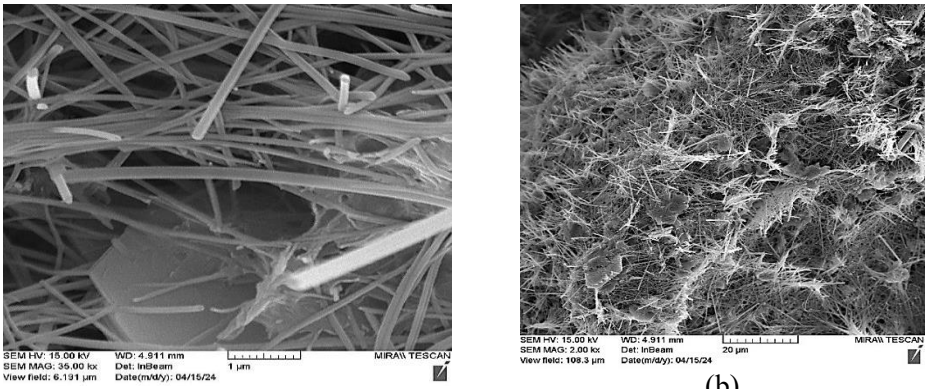

(a) (b)

Fig. 10. SEM Results: (a) 1 micro meter, (b) 20 micro meter.

BFRP-HPC Interface Pull-out Test Result

This study used ASTM D7522/D7522M [IV], a well-known standard for evaluating the tensile strength between FRP fabrics and concrete.

According to the obtained results, the maximum values of the pull-out force were converted into equivalent stress in the joint zone using the mechanical cross-sectional area of the BFRP strip (width × thickness 1.4 mm). By performing this conversion, it was found that the pull-out stresses in the different specimens were in the approximate range of 300 to 800 MPa. This difference is due to the variations in the width of the BFRP strip and the length of the limiter. A 50 mm wide specimen with a breaking load of 24.5 kN experiences a stress of about 350 MPa, whereas for a 100 mm wide specimen with a breaking load of about 46 kN, the equivalent stress is about 330 MPa. This apparent decrease in stress with increasing width is explained by the fact that the destructive force does not increase faster than the increase in the cross-sectional area, and, as a consequence, the nature of the failure becomes sensitive to the geometry of the BFRP strip. This trend suggests that increasing the FRP width does not necessarily result in an increase in the transfer stress, but rather increases the overall bandwidth of the connection.

In addition to the mechanical test results, the article discusses in detail the three-dimensional fracture behavior of the joint and the role of local phenomena. The formation of concrete bubbles observed in all tests has a significant impact on crack development and an increase in joint strength. These bubbles are formed by a combination of peeling and shear stresses and cause a mixed failure path that propagates in the concrete at an angle of approximately 30 degrees. Another important point highlighted in the article is the inadequacy of 2D models for predicting the actual behaviour of joints, since stresses and failures are entirely three-dimensional in nature. 3D modeling shows that the stress distribution in concrete consists of a confined zone near the surface and a more diffuse zone deep in the concrete, both of which play a decisive role in the ultimate strength of the joint. The results also show that changes in the width of the BFRP strip change not only the magnitude of the transmitted force, but also the failure mechanism, which is very important in the practical design of reinforced systems.

IV. Conclusions

This study investigated the effectiveness of using basalt fiber reinforced polymer (BFRP) as a core material to improve the flexural strength of high-performance concrete (HPC) beams. The main findings are summarized as follows:

1. Significant Improvement in Flexural Strength: The inclusion of BFRP in HPC beams resulted in a significant increase in flexural strength compared to the brittle behavior of samples without BFRP reinforcement. The optimal configuration with BFRP placed at 1.25 cm from the bottom achieved an increase in flexural strength by 1088% (653 kN/m^2), which demonstrates the ability of the material to increase the load-bearing capacity.

2. Ductility Enhancement: HPC beams with BFRP placed at 1.25 cm from the bottom exhibited greater ductility, with displacements up to 0.225 mm before failure, compared to the brittle behavior of samples without BFRP reinforcement (0.009 mm). This highlights the role of BFRP in improving deformation resistance and post-cracking performance.

3. Critical Role of BFRP Placement: The distance of BFRP in the tensile zone significantly affected the performance. BFRP placed at 1.25 cm from the bottom showed the best balance of flexural strength and ductility, while larger distances (e.g., BFRP placed at 2.25 cm from the bottom) reduced the effectiveness, highlighting the need for accurate placement in the load-bearing structure.

4. Practical Implications: The results show that BFRP is an effective solution for strengthening load-bearing concrete structures, especially in conditions requiring high flexural strength and ductility, such as in seismic areas or under dynamic loading conditions.

Conflict of Interest:

There was no relevant conflict of interest regarding this article.

References

I. Adak D, Sarkar M, Mandal S (2017) Structural performance of nano-silica modified fly-ash based geopolymer concrete. Construction and Building Materials, 4: 430–439. 10.1016/j.conbuildmat.2016.12.111

II. Alaa Hasan H, Neaz Sheikh M, Hadi MNS (2019) Maximum axial load carrying capacity of Fibre Reinforced-Polymer (FRP) bar reinforced concrete columns under axial compression. Structures, 19: 227–233. 10.1016/j.istruc.2018.12.012

III. ASTM C109/C109M-20 (2020) Standard test method for compressive strength of hydraulic cement mortars. ASTM International. Available from: https://store.astm.org/c0109_c0109m-20.html.

IV. ASTM D7522/D7522M-09 (2009) Standard test method for pull-off strength for FRP bonded to concrete substrate. ASTM International. Available from: https://store.astm.org/d7522_d7522m-09.html

V. Barros JAO, Ferreira DR (2008) Assessing the efficiency of CFRP discrete confinement systems for concrete cylinders. Journal of Composites for Construction, 12(2): 134–148. 10.1061/(asce)1090-0268(2008)12:2(134)

VI. Berenguer R, Lima N, Pinto L, Monteiro E, Povoas Y, Oliveira R, Lima NBD (2021) Cement-based materials: Pozzolanic activities of mineral additions are compromised by the presence of reactive oxides. Journal of Building Engineering, 41: 102358. 10.1016/j.jobe.2021.102358

VII. Beskopylny AN, Hematibahar M, Momeni K, Stel'makh SA, Shcherban EM (2025) Performance optimization of masonry mortar with marble dust, spent coffee grounds and peanut shell ash. Civil Engineering Journal, 11(3): 963–987. 10.28991/CEJ-2025-011-03-09

VIII. Chen W, Pham TM, Sichembe H, Chen L, Hao H (2018) Experimental study of flexural behaviour of RC beams strengthened by longitudinal and U-shaped basalt FRP sheet. Composites Part B: Engineering, 134: 114–126. 10.1016/j.compositesb.2017.09.053

IX. Esparham A, Vatin NI, Kharun M, Hematibahar M (2023) A study of modern eco-friendly composite (geopolymer) based on blast furnace slag compared to conventional concrete using the life cycle assessment approach. Infrastructures, 8(3): 58. 10.3390/infrastructures8030058

X. Faleschini F, Zanini MA, Hofer L, Toska K, De Domenico D, Pellegrino C (2020) Confinement of reinforced concrete columns with glass fiber reinforced cementitious matrix jackets. Engineering Structures, 218: 110847. 10.1016/j.engstruct.2020.110847

XI. Guo YC, Xiao SH, Luo JW, Ye YY, Zeng JJ (2018) Confined concrete in fiber-reinforced polymer partially wrapped square columns: axial compressive behavior and strain distributions by a particle image velocimetry sensing technique. Sensors, 18: 4118. 10.3390/s18124118

XII. GB/T 17671-2021 (2021) Test method of cement mortar strength (ISO method). National Standard of the People's Republic of China. Available from: https://www.codeofchina.com/standard/GBT17671-2021.html.

XIII. Hasanzadeh A, Vatin NI, Hematibahar M, Kharun M, Shooshpasha I (2022) Prediction of the mechanical properties of basalt fiber reinforced high-performance concrete using machine learning techniques. Materials, 15(20): 7165. 10.3390/ma15207165

XIV. Hematibahar M, Hasanzadeh A, Kharun M, Beskopylny AN, Stel'makh SA, Shcherban' EM (2024) The Influence of three-dimensionally printed polymer materials as trusses and shell structures on the mechanical properties and load-bearing capacity of reinforced concrete. Materials, 17(14): 3413. 10.3390/ma17143413

XV. Hematibahar M, Hasanzadeh A, Kharun M, Milani A, Bakhtiyari A, Namba JY, Martins CH (2025) Influence of 3D-printed fiber geometry and content on the mechanical and fracture behavior of cemented sand. Asian Journal of Civil Engineering, 26(7): 3969–3992. 10.1007/s42107-025-01412-w

XVI. Hematibahar M, Fediuk R, Momeni K, Kharun M, Bhowmik A, Romanovski V (2025) Strategic roadmap for 3D-printed reinforcement using fused deposition modeling: a state-of-the art review. Engineering Reports, 7(6): e70232. 10.1002/eng2.70232

XVII. Hematibahar M, Kharun M (2024) Prediction of concrete mixture design and compressive strength through data analysis and machine learning. Journal of Mechanics of Continua and Mathematical Sciences, 19(3): 1–21. 10.26782/jmcms.2024.03.00001

XVIII. Hematibahar M, Milani A, Fediuk R, Amran M, Bakhtiary A, Kharun M, Mousavi MS (2025) Optimization of 3D-printed reinforced concrete beams with four types of reinforced patterns and different distances. Engineering Failure Analysis Journal, 168(4): 109096. 10.1016/j.engfailanal.2024.109096

XIX. Hematibahar M, SK M, Vanus DS, M. Kharun M (2025) Comparative analysis of steel rebar and polyester fiber reinforced geopolymer concrete: mechanical properties and failure mechanisms. Journal of Mechanics of Continua and Mathematical Sciences, 20(10): 26–41. 10.26782/jmcms.2025.10.00003

XX. Hematibahar M, Vatin NI, Alaraza HAA, Khalilavi A, Kharun M (2022) The prediction of compressive strength and compressive stress-strain of basalt fiber reinforced high-performance concrete using classical programming and logistic map algorithm. Materials, 15(19): 6975. 10.3390/ma15196975

XXI. Kharun M, Alaraza HAA, Hematibahar M, Al Daini R, Manoshin A (2022) Experimental study on the effect of chopped basalt fiber on the mechanical properties of high-performance concrete. AIP Conference Proceedings, 2559: 050017. 10.1063/5.0099042

XXII. Kharun M, Koroteev D (2018) Effect of basalt fibres on the parameters of fracture mechanics of MB modifier based high-strength concrete. MATEC Web of Conferences, 251: 02003. 10.1051/matecconf/201825102003

XXIII. Saribiyik A, Abodan B, Balci MT (2021) Experimental study on shear strengthening of RC beams with basalt FRP strips using different wrapping methods. Engineering Science and Technology, an International Journal, 24(1): 192–204. 10.1016/j.jestch.2020.06.003